PHYSICAL REVIEW B VOLUME 61, NUMBER 3 15 JANUARY 2000-I

Layer perfection in ultrathin InAs quantum wells in GaAs(001)

J. A. Gupta,* S. P. Watkins, and E. D. Crozier
Department of Physics, Simon Fraser University, Burnaby, British Columbia, Canada V5A 1S6

J. C. Woicik
National Institute of Standards and Technology, Gaithersburg, Maryland 20899

D. A. Harrison† and D. T. Jiang
Department of Physics, Simon Fraser University, Burnaby, British Columbia, Canada V5A 1S6

I. J. Pickering
Stanford Synchrotron Radiation Laboratory, P.O. Box 4349, MS 69, Stanford, California 94309

B. A. Karlin
National Institute of Standards and Technology, Gaithersburg, Maryland 20899
(Received 30 March 1999; revised manuscript received 2 August 1999)

X-ray standing wave (XSW), x-ray diffraction, and photoluminescence (PL) measurements were used to assess the layer perfection and positions of 1 and 1/2 monolayer (ML) InAs quantum wells buried in GaAs(001). Local structure in the 1-ML films was evaluated using x-ray absorption fine structure (XAFS) measurements. Growth temperature effects were studied in a series of samples produced by metal organic vapor phase epitaxy (MOVPE) between 400 and 600 °C. The XSW coherent position of the In atoms decreases with increasing temperature in the 1-ML samples, and the optimal growth temperature is near 550 °C, as evidenced by the coherent position of 1.15 ± 0.02 and the relatively high coherent fraction of 0.72 ± 0.08. With decreasing growth temperature the XSW measurements may suggest segregation of In atoms, which results in an incorporation of the In into multiple layers. The segregation appears to be reduced at the higher temperatures due to the favorable kinetic conditions created in the MOVPE environment. Low-temperature PL measurements indicate that the sharpest and most intense In-excitonic emission is obtained from the 1-ML sample grown at 530 °C. For the $\frac{1}{2}$-ML samples, growth temperatures of 400 and 600 °C produce similar standing wave results, although the PL reveals the higher temperature sample to be of far superior quality, due to excessive carbon incorporation at 400 °C. In-As bond-length distortions found in the XAFS measurements agree with a macroscopic elastic description of the pseudomorphic epitaxy.

I. INTRODUCTION

Quantum wells of InAs in GaAs(001) constitute one of the most highly-strained III-V semiconductor heterostructures. The ~7% lattice mismatch results in a critical thickness for layer-by-layer epitaxy of only ~1.5 ML, making this system ideal for the study of fundamental materials issues.[1–6] With In depositions of only fractions of a monolayer, sharp and intense In-excitonic photoluminescence (PL) emission has been observed.[5–11] Additionally, very recent theoretical[12] and experimental[13] studies have re-emphasized the technological promise of InAs single quantum wells for highly efficient excitonic lasing.

For these ultrathin InAs layers buried beneath a GaAs capping layer, the determination of the In local structure is a nontrivial task. During the epitaxial growth, researchers have observed segregation of the In atoms during the deposition of the topmost GaAs layer[14–26] using a variety of surface-analytical, optical and structural techniques. Suppression or elimination of this In/Ga exchange reaction remains one of the challenges for the successful fabrication of perfect δ layers. Based on an earlier suggestion,[14] Brandt *et al.*[6] developed a technique for circumventing this dilemma by ''flashing off'' the segregated In atoms in molecular beam epitaxy (MBE). X-ray standing wave (XSW) measurements on samples produced by this technique were interpreted in terms of In segregation, from which it was postulated that the ''flash off'' was effective in reducing the segregation efficiency to about 25%.[1]

In the present paper, we use complementary short-range-order [polarization-dependent x-ray absorption fine structure (XAFS)] and long-range-order techniques [double-crystal x-ray diffraction (XRD), back-reflection XSW)] including element specificity (XAFS, XSW) to obtain the structure of metalorganic vapor phase epitaxy (MOVPE)-grown InAs quantum wells. This permits a characterization of the In atomic distribution and provides a structural basis for understanding the optical (PL) properties of the material. A series of 1-ML and $\frac{1}{2}$-ML samples were prepared to allow a study of the effect of growth temperature on the structural and optical quality of the films and to provide insight into the most suitable conditions for producing ''perfect'' layers, which might be employed in novel optoelectronic devices.

II. EXPERIMENT

Epitaxy was performed in a Thomas Swan vertical MOVPE reactor at 50 Torr. Semi-insulating vertical gradient

0163-1829/2000/61(3)/2073(12)/$15.00 PRB 61 ©2000 The American Physical Society

freeze GaAs(001) epiready substrates were used with no additional cleaning. Following annealing under tertiarybutylarsine (TBA's) at 580 °C, a GaAs buffer layer was grown using triethylgallium (TEGa) and TBA's with flow rates of 8.07 μmole/min and 198 μmole/min, respectively. Atomic force micrographs of buffer layers produced in this way were very smooth and exhibited broad, well-defined atomic terraces approximately 0.1 μm wide. Each sample was then allowed to equilibrate at the desired growth temperature T_g. GaAs barrier layers of thickness $\sim$100 Å were deposited above and below the InAs layer that was also grown at T_g using trimethylindium at 1.98 μmole/min and TBA's at 198 μmole/min, yielding a growth rate of approximately 1 ML per 3 s. For the PL samples an additional GaAs cap layer ($\sim$1900 Å) was deposited at 580 °C.

High-resolution x-ray diffraction with a Cu anode ($\lambda = 1.54$ Å) and a double crystal channel-cut monochromator was used to characterize the final structures. Rocking curves were obtained by scanning in angle, θ, about the Bragg angle, θ_B, where $\lambda = 2d_s \sin\theta_B$, in terms of the diffraction plane spacing d_s.

XSW measurements were made at the National Institute of Standards and Technology beamline X24A at the National Synchrotron Light Source, Brookhaven National Laboratory. The monochromator consisted of a pair of Si(220) crystals. Standing waves were produced within the GaAs sample crystals and modulated in phase by scanning in energy through the GaAs (004) sample back-reflection at normal incidence. Fluorescence yield data were obtained using a single-element Ge detector positioned at a right angle to the incident beam. A Be detector window of thickness 50.8 μm was used to reduce the intensity of the Ga and As L emission with respect to the In-L fluorescence signal. Reflectivity measurements were made by recording the back-reflected photon intensity with a Ni mesh upstream from the sample.

Low-temperature photoluminescence measurements were performed at 1.6 K using Ar-ion laser excitation. The spectra were recorded with a Fourier transform interferometer.

XAFS measurements were made at beamline 4-2 of the Stanford Synchrotron Radiation Laboratory with the storage ring operating at an electron energy of 3 GeV and a stored current in the range of 100-65 mA. Data were collected with a double-crystal monochromator using Si(220) crystals, with an entrance slit width of 1 mm and no beam focusing. The collimating vertical slit width was 0.3 mm to align the beam footprint on the sample. In K-edge ($E_0 = 27940$ eV) XAFS was measured in the glancing incidence geometry ($\theta = 0.2°$) using a SSRL grazing incidence x-ray absorption spectroscopy stage. This permitted polarization-dependent measurements with the electric vector of the x-rays oriented parallel $E_\parallel$, or perpendicular $E_\perp$, to the substrate surface. The incident angle is slightly greater than twice the critical angle ($\theta_C = 0.090°$ at $E_0 + 200$ eV) to allow the penetration of the incident beam to the depth of the In atoms. The incident, I_0, and reflected I_1, photon intensities were measured using Ar-filled ionization chambers. In K_α-fluorescence emission was measured using a 13 element Ge detector, with two Al plates, thickness 0.75 mm, in front of the detector to reduce the total incoming count rate contribution from the Ga and As fluorescence.

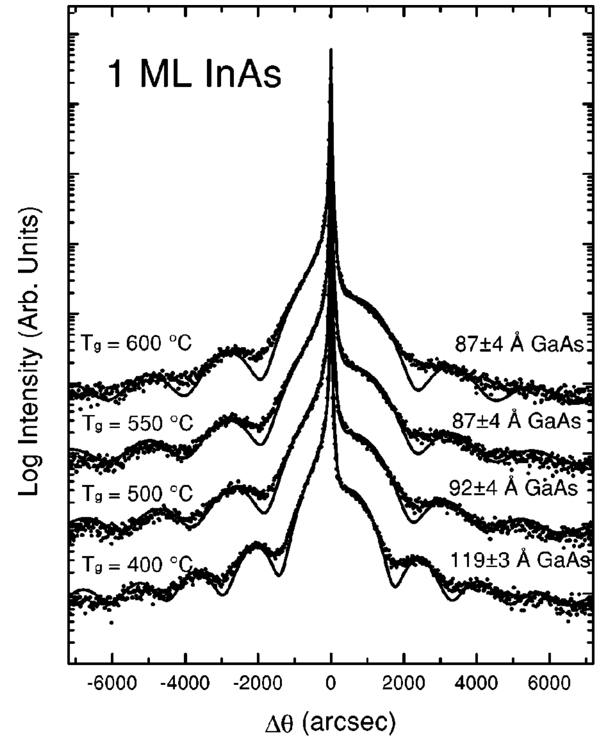

FIG. 1. X-ray rocking curve data obtained near the GaAs(004) symmetric substrate reflection, for $\Delta\theta = \theta - \theta_B$. The data for the 1-ML samples with several growth temperatures are indicated by points. Solid lines denote the results of dynamical simulations with the GaAs cap thicknesses indicated, as described in the text.

III. RESULTS AND ANALYSIS

A. X-ray diffraction

High resolution XRD data for 1-ML and $\frac{1}{2}$-ML samples are shown in Figs. 1 and 2. The experimental curves are compared to simulations using the dynamical diffraction theory.[27] These simulations are based on a 3-layer model consisting of the GaAs substrate, a single In-containing layer, and a GaAs cap layer. For the 1-ML samples, the thickness of the strained InAs layers used in the simulations was 3.25 Å , as predicted by the macroscopic elastic theory (MET),[28] assuming single layers of In atoms and coherency of the InAs layers with the GaAs substrate. For the $\frac{1}{2}$-ML samples the MET was also used, assuming single $In_xGa_{1-x}As$ layers, as will be discussed. From the interference fringes it is possible to obtain an accurate measurement of the GaAs cap thickness, as indicated. However, this technique is slightly less sensitive to the distribution of In atoms in the quantum well layer, particularly in the case of these sandwich structures with very thin GaAs caps. Although the high-resolution XRD data can, in principle, be used to determine the total amount of incorporated indium, in practice the experimental resolution is somewhat limited. From Fig. 1, it is clear that the In content in the nominally 1-ML samples is very close to a single monolayer. It was pointed out[1] that complementary information may be obtained by using XSW in addition to XRD.

B. XSW analysis

Figure 3 shows the reflectivity (lower curve) obtained using the XSW apparatus for a bulk GaAs reference crystal

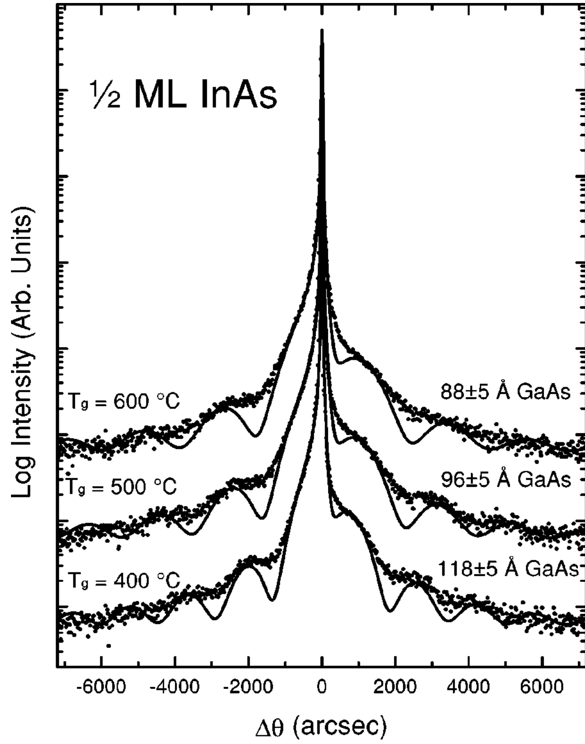

FIG. 2. X-ray rocking curve data obtained near the GaAs(004) symmetric substrate reflection, for $\Delta\theta=\theta-\theta_B$. The data for the $\frac{1}{2}$-ML samples with several growth temperatures are indicated by points. Solid lines denote the results of dynamical simulations with the GaAs cap thicknesses indicated, as described in the text.

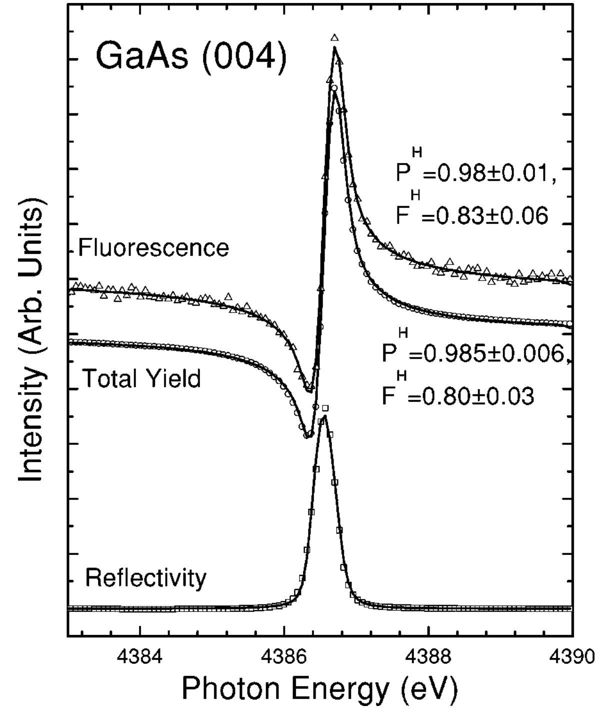

FIG. 3. Photon-energy dependence of the reflectivity (bottom curve) for a reference epiready GaAs crystal near the GaAs(004) Bragg back-reflection. The XSW patterns obtained by measuring the total electron yield and the Ga and As *L*-fluorescence yields are shown in ascending order, with fit parameters as indicated. The spectra were offset for clarity.

near the (004) back-reflection condition. It is important to note that this epiready crystal was measured with no cleaning or processing. The XSW patterns (top curves) were obtained using the total electron yield (TEY), and the Ga and As L-fluorescence yields (FLY). The standing wave in the crystal results from the superposition of the incident and back-reflected traveling waves[29] and has the periodicity of the crystal lattice planes with diffraction vector $\vec{H}$. At the low-energy side of the Bragg reflection the nodes of the standing wave lie on the substrate planes. As the phase shifts throughout the Bragg peak the wavefield moves continuously until the antinodes lie on the substrate planes at the high-energy side.[30] The TEY and FLY spectra, shown in the top curves of Fig. 3 are proportional to the absorption of the atoms in the field of the standing wave. From this response the spatial distribution of a given type of atom may be deduced.

The yield from the standing wave measurement is written[29] in terms of the coherent fraction F^H, which measures the δ-like nature of the atomic distribution perpendicular to the diffracting planes, and the coherent position P^H, which measures the position of a particular type of atom relative to the substrate planes, normalized by the diffraction plane spacing, d_s. (For a single atom in bulk $P^H=1$.) The yield Y^H is

$$Y^H=Y^0[1+R+2\sqrt{R}F^H\cos(\alpha-2\pi P^H)]. \quad (1)$$

Here, R and α denote the reflectivity and phase as given by the dynamical theory of x-ray diffraction,[29] and Y^0 is proportional to the beam flux. Thermal vibrations may be taken into account by a Debye-Waller factor e^{-M}, which decreases the measured value of F^H to approximately 0.9 in GaAs.[31] For the GaAs reference crystal the expected values are $P^H=1.0$, and $F^H=e^{-M}$. The measured values (Fig. 3) obtained using both types of emission (TEY, FLY) agree with one another and are close to the expected values. Lee *et al.* measured values of $P^H=1.00\pm0.01$ and $F^H=0.81\pm0.01$ for their GaAs buffer layer[3] in good agreement with the present results. With our experimental setup, the takeoff angle viewed by the Ge detector allowed the measurement of fluorescent photons originating from deep within the crystal and reduced the extinction problem.[32] Also, for the relatively low-photon energies employed in this paper the TEY signal should approximate a bulk site close to the crystal surface,[33] and so the measured values are due to atoms on bulk sites within the crystal. This suggests that the Debye-Waller factor may be slightly smaller than 0.9 in these samples.

Figures 4 and 5 show the XSW data for 1- and $\frac{1}{2}$-ML InAs samples prepared at a series of growth temperatures. From the MET,[28] a single InAs ML in GaAs is expected to have $P^H=1.146$ under pseudomorphic conditions.[2] Comparing the raw data of Figs. 4 and 5 with Fig. 3 it is clear that the In atoms do not occupy the same positions as the substrate Ga atoms. Our best 1-ML sample, structurally, is the one with $T_g=550\,^\circ$C, having an ideal coherent position and the highest F^H. $\frac{1}{2}$-ML samples grown at 400 and 600 °C have similar positional values to one another and high values of F^H. Notice the more bulklike characteristics of the data for the $\frac{1}{2}$ ML.

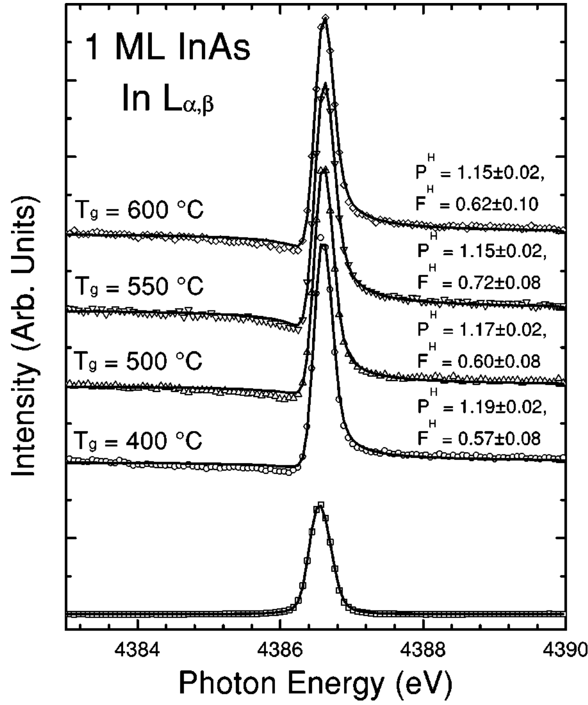

FIG. 4. Photon-energy dependence of the reflectivity (bottom curve) and the In-L fluorescence yield near the GaAs(004) Bragg backreflection condition for a series of 1-ML InAs samples, with growth temperatures as indicated. The solid lines are the best fits to the data points. The spectra were offset for clarity.

In a previous XSW measurement of a $\frac{1}{2}$-ML InAs film in GaAs,[5] it was found that the measured P^H was consistent with a single $In_xGa_{1-x}As$ alloy layer, similar to the result obtained by Woicik *et al.* for an alloy layer grown by MBE.[4] The unstrained lattice constant a_f for such a layer is determined from Vegard's law as

$$a_f = x a_{InAs} + (1-x) a_{GaAs}, \tag{2}$$

where $a_{GaAs} = 5.6532$ Å and $a_{InAs} = 6.0584$ Å are the bulk lattice constants. For pseudomorphic epitaxy, the lattice constant of the alloy layer in the plane, $a_\parallel$, is equal to the value for GaAs, from which the lattice constant perpendicular to the interface plane, $a_\perp$, is determined using the MET.[2] The lattice strains parallel, $\epsilon_\parallel$, and perpendicular, $\epsilon_\perp$, to the interface are given by $\epsilon_\perp = (a_\perp - a_f)/a_f$ and $\epsilon_\parallel = (a_\parallel - a_f)/a_f$. These are related through the elastic constants C_{11} and C_{12} as

$$\epsilon_\perp = -2\left(\frac{C_{12}}{C_{11}}\right)\epsilon_\parallel . \tag{3}$$

For the $In_xGa_{1-x}As$ alloy the elastic constants are given by the concentration-weighted elastic constants of both materials[5]

$$C_{11}^f = x C_{11}^{InAs} + (1-x) C_{11}^{GaAs},$$

$$C_{12}^f = x C_{12}^{InAs} + (1-x) C_{12}^{GaAs}. \tag{4}$$

The In mole fraction of a layer with a given P^H can then be found using

$$a_\perp = a_f - 2\left[\frac{x C_{12}^{InAs} + (1-x) C_{12}^{GaAs}}{x C_{11}^{InAs} + (1-x) C_{11}^{GaAs}}\right](a_{GaAs} - a_f), \tag{5}$$

and using the standing wave result $a_\perp = P^H a_{GaAs}$. Using this method we find the following values of x for the $\frac{1}{2}$-ML samples 0.63 ± 0.14, 0.56 ± 0.14, and 0.69 ± 0.14, in order of increasing T_g.

In order to clarify the mechanism producing the higher-than-ideal coherent positions in the 1-ML samples with the lowest T_g values, we consider the possibility of In atoms occupying multiple sites in the crystal. If the In atoms occupy n positions (P_i^H) relative to the diffraction planes, then P^H and F^H may be written[29]

$$F^H = (G_H^{c\,2} + G_H^{s\,2})^{1/2}, \tag{6}$$

and

$$P^H = \frac{1}{2\pi}\tan^{-1}\left(\frac{G_H^s}{G_H^c}\right) + \begin{cases} 0.5, & \text{if } G_H^c < 0 \\ 0 & \text{otherwise,} \end{cases} \tag{7}$$

where the cosine term G_H^c has the form

$$G_H^c = \sum_{i=1}^{n} c_i \cos(2\pi P_i^H), \tag{8}$$

and the sine term G_H^s is

$$G_H^s = \sum_{i=1}^{n} c_i \sin(2\pi P_i^H). \tag{9}$$

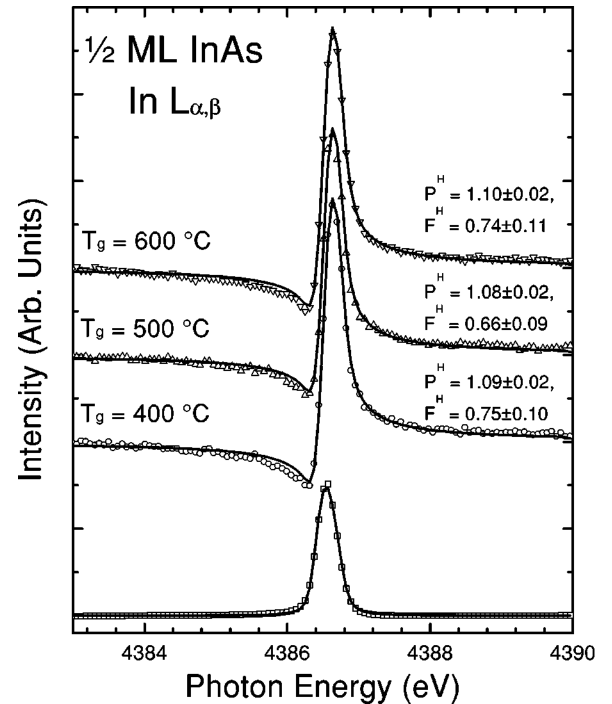

FIG. 5. Photon-energy dependence of the reflectivity (bottom curve) and the In-L fluorescence yield near the GaAs(004) Bragg backreflection condition for a series of $\frac{1}{2}$-ML InAs samples, with growth temperatures as indicated. The solid lines are the best fits to the data points. The spectra were offset for clarity.

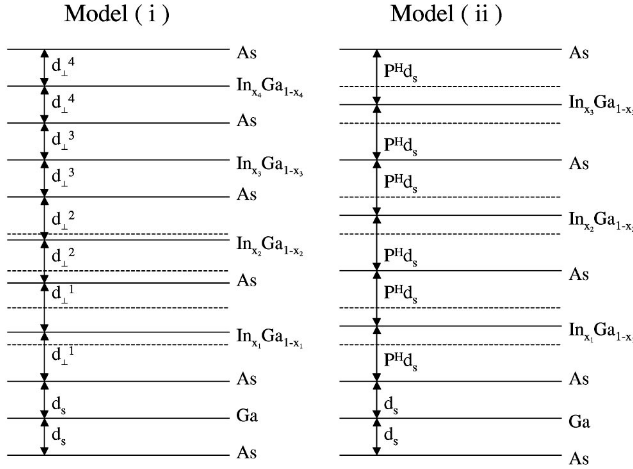

FIG. 6. The distribution of In atoms relative to the GaAs(004) planes according to the two models described in the text. In model (i) the distance $d_\perp^i$ between each cation plane and its corresponding As plane is a function of the In concentration x_n. For model (ii) the spacing is the same for all planes, independent of In content.

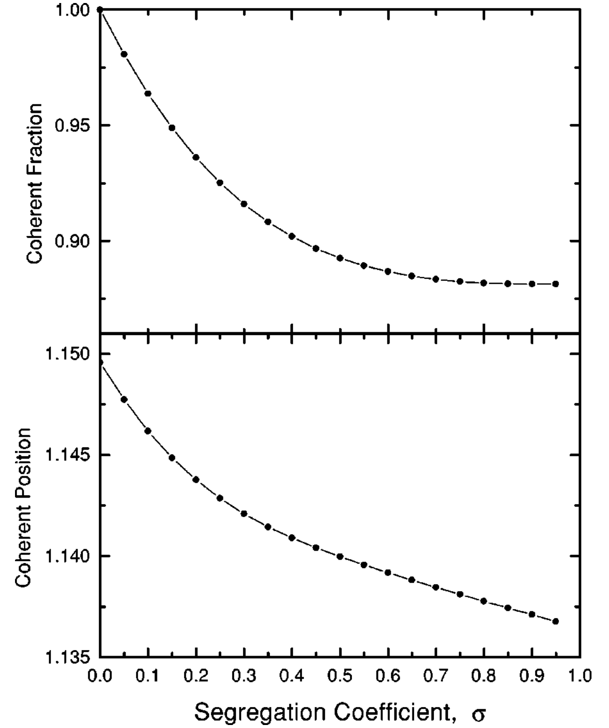

FIG. 7. X-ray standing wave parameters as a function of segregation coefficient σ predicted by model (i) described in the text, with 1 ML total In coverage.

The coefficients in these expressions satisfy the normalization $\Sigma_{i=1}^{n} c_i = 1$, where c_i denotes the relative population of the position P_i^H.

Previous XSW measurements[1] were interpreted assuming surface segregation of In atoms during the growth of the GaAs cap layer. We consider the results that might be obtained in an XSW measurement of an InAs layer buried in GaAs(001) including this process, where the total In content is 1 ML. It is very important to note that a single XSW measurement provides only one Fourier component of the In distribution. This presents a uniqueness problem when one attempts to infer additional information in this way, although the measured values do place some constraints on the structural possibilities.

The issue of segregation of third-column atoms in the growth of III-arsenide heterostructures has been addressed in some depth by Guille, Moison *et al.*[14,15] A simple model was proposed[14] in which the segregation is characterized by an efficiency coefficient σ. When the first monolayer of GaAs is deposited on the InAs monolayer (layer 1), a fraction σ of the In atoms segregate to the surface, burying the same fraction of the deposited Ga monolayer. The process continues during the deposition of subsequent GaAs layers. We consider two possibilities: (i) Each group III layer consists of an In,Ga alloy, with the composition of sequential layers graded in the growth direction. The composition of the nth layer, $In_{x_n}Ga_{1-x_n}As$, is x_n and

$$x_n = (1-\sigma)\sigma^{n-1}. \tag{10}$$

and the strained lattice constant of each layer is found from Eqs. (2)–(5). In this scenario the In atoms are located at $\frac{1}{2}$ the lattice constant of the strained layer, which is a function of x_n. The other possibility is: (ii) Each group III layer contains In and Ga atoms as above, with the In atoms arranged in equidistant ''terraces'' or islands. For each layer the tetragonally distorted InAs cell is expanded 14.6% in the (001) direction compared to GaAs. This is the scheme used in Ref. 1. An illustration of the two models appears in Fig. 6. It should be noted that (i) implicitly makes a virtual crystal approximation by assuming that both In and Ga atoms reside in the same cation plane. It is well known that the In-As and Ga-As bond lengths do not deviate significantly from their native values in the ternary alloy,[34,35] and that the atoms do not occupy the virtual crystal positions. Model (i) is to be considered as a first approximation in lieu of a more complete description.

Model (ii) assumes terracing of the In atoms, and neglects edge effects, which are likely present at the boundaries between the InAs and the surrounding GaAs. Additionally, this assumes equal strain in all InAs layers in spite of the differences in In content. In this respect model (i) is somewhat more realistic.

We have estimated the possible XSW parameters using both models. In case (i), with a given σ, the lattice constant for the nth layer was estimated using Vegard's law and equation 10, which gives the bulk lattice constant. The effect of strain is included using MET as discussed previously.

If the (004)-plane spacing between the ith In,Ga layer and the corresponding As-plane is denoted by $d_\perp^i$, then the total distance of the nth layer from the last As-plane of the substrate is

$$d^n = 2\sum_{i=1}^{n-1} d_\perp^i + d_\perp^n. \tag{11}$$

These positions may then be substituted into Eqs. (8) and (9) from which F^H and P^H are determined.

The results for a range of segregation coefficients are shown in Figs. 7 and 8 for (i) and (ii), respectively. For the model (i) in which the segregation produces a graded $In_xGa_{1-x}As$ alloy, the theoretical XSW parameters P^H and

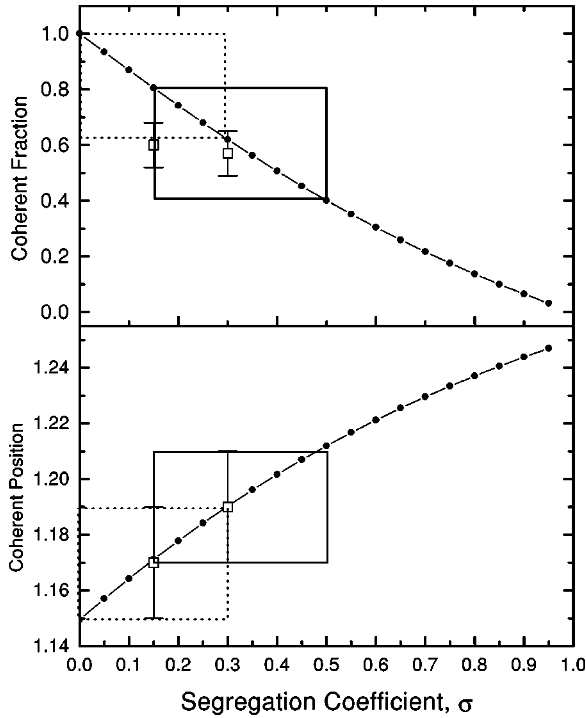

FIG. 8. X-ray standing wave parameters as a function of segregation coefficient σ predicted by model (ii) described in the text. In the bottom half of the figure the experimental XSW coherent positions (small hollow squares) are compared with the values of the segregation coefficient σ, which might produce the measured P^H. The solid and dashed rectangles are used to indicate the range of possible values of σ for the 1-ML samples grown at 400 and 500 °C, respectively. In the top half of the figure the corresponding values of F^H are indicated, as well as the experimental values.

F^H are found to decrease with increasing segregation, but remain close to the values for the ideal ML. It is clear from the figures that only (ii) can explain the experimental results in which $P^H > 1.15$. For samples grown at 400 °C and 500 °C, the XSW coherent positions are found to be consistent with $\sigma = 0.30$, and $\sigma = 0.15$, respectively, as indicated. Moreover, the experimental values of F^H are consistent with this interpretation, if the Debye-Waller factor is included. Let us reemphasize that this interpretation of the XSW data is not entirely conclusive.

Considering the relationship between the data and the island model, the results are somewhat surprising; the segregation coefficients inferred from the data are found to be *greater* for the samples grown at the lowest temperatures. Since Giannini *et al.* measured only one sample using XSW,[1] the effect of changing the growth temperature was not discussed. They found $P^H = 1.17 \pm 0.02, F^H = 0.58 \pm 0.07$ which was related to a segregation coefficient of $\sigma \approx 0.25$ when the structure was grown by MBE with the flashoff technique. In their experiment, the InAs ML and the first 5 ML of the GaAs cap were deposited at 420 °C. The temperature was then raised to 540 °C to desorb the segregated In. Finally, 300 Å of GaAs were deposited at 540 °C.

In studies of indium segregation in GaAs(001)/InAs/GaAs structures in the literature, thermodynamic and kinetic models have been suggested to describe the process. Guille, Moison *et al.* have carried out detailed *in-situ* studies during the growth of MBE films, both δ layers and ternary alloys, grown at 420 (Ref. 14) and 480 °C.[15] In the thermodynamic model,[15] the surface, x_s, and bulk, x_b, concentrations of In are related by the expression:

TABLE I. Temperature dependence of GaAs growth rate, from the GaAs cap thicknesses determined by XRD.

Temperature (°C)	Growth rate (μm/hr)
400	1.94±0.07
500	2.42±0.12
550	2.41±0.11
600	2.42±0.13

$$\ln\left(\frac{x_s}{1-x_s}\right) + \frac{E_s}{kT} = \ln\left(\frac{x_b}{1-x_b}\right). \tag{12}$$

A modified expression takes into account the lattice mismatch between InAs and GaAs. Experimentally the segregation energy E_s, was found to be near 0.15 eV.

Other experiments[18–23] have found that In segregation increases with increasing growth temperature. However, Eq. (12) predicts the opposite behavior. A kinetic model[36] has successfully reproduced the results at fixed temperature while accounting for the observed increase with growth temperature.[26] The incident As flux has also been shown to affect the segregation,[25] and might be included in an even more complete model.

If our XSW data were interpreted using model (ii) as discussed above, then this would indicate increasing In segregation with decreasing T_g. This disagrees with the experimental evidence for MBE growth obtained by other means[18–23] due to differences in the growth conditions between MBE and MOVPE. Results for MBE-grown samples[37] have indicated that the growth temperature of the GaAs barriers also plays a pivotal role.

For the 1 ML samples grown at 550 °C and 600 °C the XSW results indicate near ideal In distributions, particularly in the former. We attribute this to the favorable conditions created in the MOVPE environment.[16] Let us address the requirements for minimal segregation suggested by other authors.

As shown in Table I, the GaAs cap growth rate is independent of temperature for 500 °C$\leqslant T_g \leqslant$600 °C. This is indicative of mass-transport-limited (MTL) growth.[38] Gérard *et al.*[17] suggested that the segregation process may be minimized by suitable adjustment of the kinetics during the caplayer growth. In the MTL regime the growth may be less susceptible to a kinetic rearrangement of group-III atoms, allowing a reduction in the In-Ga exchange reaction. At 400 °C, which is in the surface-kinetic-limited regime, the growth kinetics may play a larger role. A strong temperature dependence in the surface reconstruction during growth has been observed.[39] This results from the incomplete decomposition of the TBA's molecules at the lower temperatures, which may contribute to the apparent enhancement in the segregation under these conditions.

Guille *et al.*[14] suggested that very high-GaAs growth rates could beat the In-Ga exchange rate, although this was not the case for up to 0.5 μm/h. Recent results[25] for MBE-grown

$In_xGa_{1-x}As/GaAs$ structures at 5.1 μm/h and 500 °C have noted the reduction in the In segregation due to the rapid surface coverage. At our higher temperatures we have a GaAs growth rate of 2.4 μm/h, which may be sufficient to discourage segregation. At lower temperatures the reduced GaAs growth rate allows the segregation process to occur more prominently.

Using reflectance difference spectroscopy, time-resolved studies were carried out during the growth of these quantum well structures.[39] Although it was noted that segregation may occur during GaAs overgrowth, the effect was not completely pronounced in the data. In contrast, clear evidence of In segregation was observed during atomic layer epitaxy (ALE) growth[24] which has a much higher cation surface mobility than conventional MOVPE. Recall that in the atomic layer mode the incident group-III molecules are not accompanied by a group-V flux, and are thus much more mobile on the surface. This mobility produces the smooth interfaces that are associated with the technique. Unfortunately, the lack of As overpressure can lead to enhanced exchange reactions between incoming Ga atoms and the underlying In.[15,23] While ALE produces interfaces that are highly uniform and smooth[21] they suffer from reduced abruptness. We have found that In segregation cannot be eliminated in the ALE growth for any usual growth temperature.[40]

We conclude that the combination of growth in a MTL regime, high-growth rate, and low cation surface mobility aid in reducing the effects of segregation in the 1-ML structures produced at the higher temperatures. For the samples grown at lower temperatures, the XSW data may be indicative of enhanced In segregation. This could be due to surface kinetics effects: lower As coverage on the growing surface, and the lower GaAs growth rate. Although these factors are a direct consequence of the reduced temperature, the temperature itself is not the important parameter *per se.*

Alternatively, it is possible that the nominally 1-ML samples grown at the lowest temperatures contain more than one layer of In atoms. We can consider this case by supposing that the films contain one perfect In layer, with additional In located in a second layer above the first. As in the previous discussion, the In atoms in the second layer could be arranged in an In,Ga alloy layer, or in a ''terraced layer.'' In the alloy layer the In-As planar distance would be given by Eqs. (2)–(5). In the ''terraced layer'' the In-As planar distance would be expanded 14.6% in the (001) direction compared to GaAs.

Figure 9 shows the predicted values for the XSW coherent position and coherent fraction which would be obtained for two-layer systems of this type as a function of second layer In coverage. The XSW parameters were determined using Eqs. (6)–(9). Notice that the two models converge at the endpoints, i.e., for exactly 1 ML of In or exactly 2 ML of In. For intermediate coverages the coherent position is very similar between the two cases, and varies roughly linearly with second-layer coverage. The greatest discrepancies between the two models occurs for a second-layer coverage of 61%, which is well beyond the possibilities for our measured values of P^H.

For the nominally 1-ML samples grown at 400 and 500 °C, the measured values of P^H were 1.19±0.02 and 1.17 ±0.02, respectively. In Fig. 9 it is shown that these values

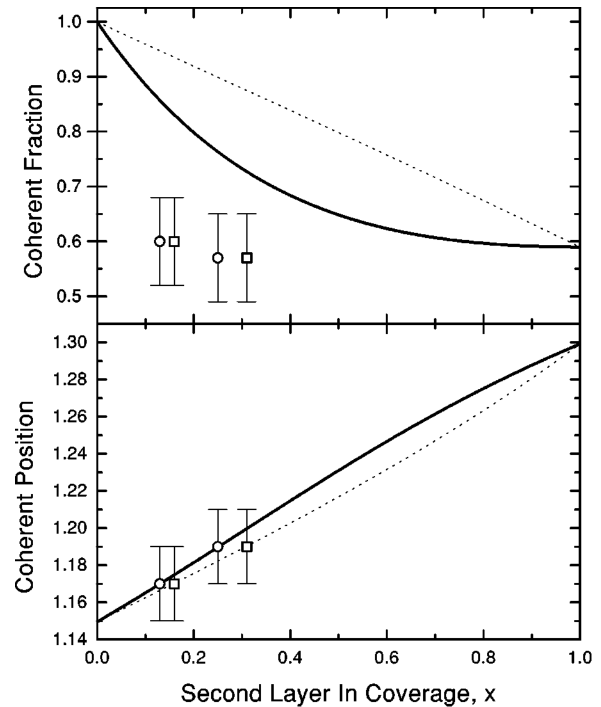

FIG. 9. X-ray standing wave parameters for greater than 1 ML of In coverage, as a function of In second-layer coverage x. In the bottom half of the figure the experimental XSW coherent positions for the 1-ML samples grown at 400 and 500 °C (hollow squares) are compared with the values of the second-layer coverage x, which might produce the measured P^H values using the alloy model (dashed line). The hollow circles indicate the correspondence between the experimental results and the terrace model (solid line). In the top half of the figure the corresponding values of F^H are indicated, as well as the experimental values.

can be associated with second-layer In coverages of 0.31 and 0.16 using the alloy model. The terrace model gives the values 0.25 and 0.13, for the 400 and 500 °C samples, respectively. In the figure the correspondence between each of these models and the experimental P^H values are indicated. From the measured P^H values it is not possible to determine which model might actually describe the situation.

On the other hand, the two models show larger differences in the predicted values of F^H. For increasing second-layer In coverage the alloy model predicts a nearly linear decrease in the measured coherent fraction. The terrace model, in which the two In layers are separated by a larger distance, shows a more dramatic decrease with increasing second-layer coverage.

From the top curves of Fig. 9, it is clear that the measured values of F^H are significantly lower than the values predicted by either model. By including thermal effects through a Debye-Waller factor of 0.9 (Ref. 31) the discrepancy between the experimental and predicted values is decreased somewhat, but still suggests a certain degree of random structural disorder in the films. Recall that our XSW measurements for a bare GaAs wafer suggested that the Debye-Waller factor may actually be closer to 0.8. Even this value cannot completely account for the measured coherent fractions.

It should be pointed out that this interpretation would suggest that the In coverage decreases with increasing growth

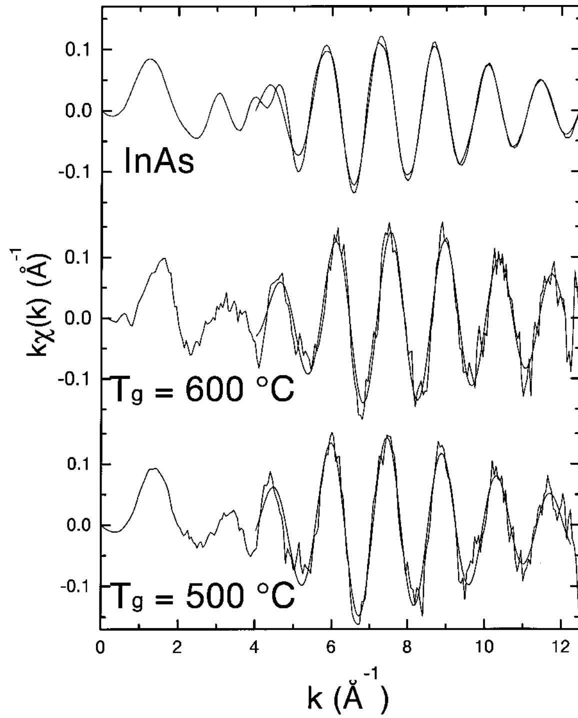

FIG. 10. k-weighted In K-edge XAFS, $k\chi(k)$, with $E_{\|}$- polarization, from 1-ML InAs films and growth temperatures as indicated. The top spectrum was obtained using an InAs reference powder in transmission. Superimposed on the data are the fits to the Fourier filtered first-shell contributions, which correspond to the In-As near-neighbor bond lengths.

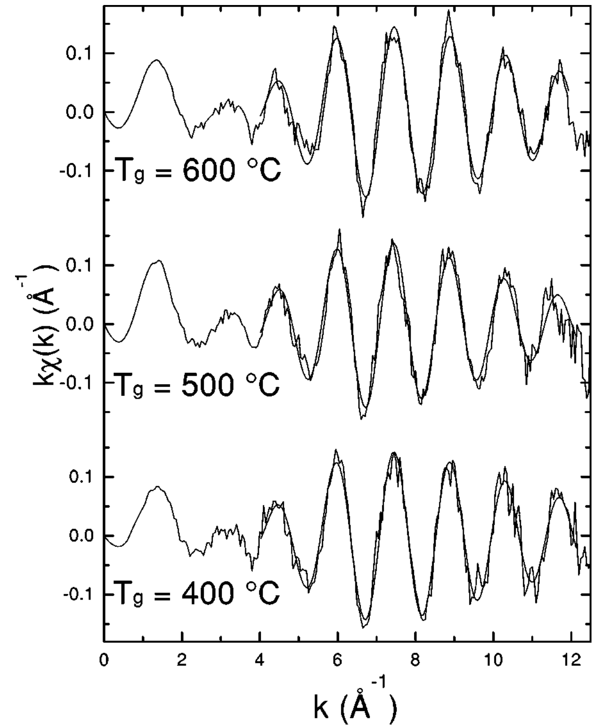

FIG. 11. k-weighted In K-edge XAFS, $k\chi(k)$, with $E_{\perp}$-polarization, from 1-ML InAs films and growth temperatures as indicated. Superimposed on the data are the fits to the Fourier filtered first-shell contributions, which correspond to the In-As near-neighbor bond lengths.

temperature. In studies of InAs homoepitaxy, Watkins *et al.* observed the opposite behavior, i.e., an increasing growth rate with increasing temperature.[41] For the ML samples the heteroepitaxial strain affects the In incorporation, so the homoepitaxy results do not entirely preclude the possibility of excess In in these films.

C. XAFS analysis

In order to resolve details of the local structure of the In atomic distribution, we consider the results of XAFS measurements in both the $E_{\|}$ and $E_{\perp}$ orientations. The XAFS, χ, was separated from the In K-fluorescence data using the AUTOBK program.[42] This involved pre-edge background removal using a linear fit; normalization to the edge jump to put the data on a per atom basis; and removal of the postedge background. AUTOBK uses a fourth-order polynomial spline with knots equally spaced in k space[42] to minimize the low R background in the Fourier transform of $k\chi(k)$, where k is the photoelectron wave number: $k=\sqrt{2m(E-E_0)}/\hbar$.

Figures 10 and 11 show the normalized XAFS $k\chi(k)$ data for 1-ML samples in both polarizations, as well as for an InAs reference powder.[43] The corresponding Fourier transforms for the data are shown in Fig. 12. In all cases a 10% Gaussian window was used in the transformations, which were taken from approximately 0.7 to 12 Å $^{-1}$.

The XAFS is expressed as[44]

$$\chi(k)=\sum_i B_i(k)[3\cos^2(\theta_i)]\sin[2kR_i+2\delta(k)+\phi_i(k)], \tag{13}$$

where the sum is taken over all atoms i, located at distances R_i from the absorbing atom. The factor $\cos^2(\theta_i)$ is related to the polarization dependence of the K-shell XAFS in the dipole approximation, where θ_i is the angle between the electric vector and the bond between the absorber and the backscatterer. Phase shifts, $\delta(k)$, and $\phi_i(k)$ arise from the interaction between the photoelectron with the absorber and the backscatterer, respectively.

The amplitude function $B_i(k)$ is

$$B_i(k)=\frac{N_i}{kR_i^2}S_0^2F_i(k)e^{-2R_i/\lambda_i(k)}e^{-2k^2\sigma_i^2}, \tag{14}$$

where N_i is the number of atoms of type i located at an average distance R_i from the absorber. S_0^2 is the passive electron factor describing the overlap between the wavefunctions of the electrons in the absorbing atom before and after the ejection of the core photoelectron ($S_0^2<1$). The backscattering amplitude of atom i is given by $F_i(k)$, $e^{-2k^2\sigma_i^2}$ is the XAFS Debye-Waller factor where σ_i^2 is the mean-square relative displacement about the average distance R_i, including thermal and static disorder, and $\lambda_i(k)$ is the mean free path of the photoelectron.

In order to analyze the experimental data we have used the theoretical package FEFF6b (Ref. 45) to create a model for a single InAs layer buried in GaAs. Using the strained lattice parameters of the InAs cell from the MET, we simulated the XAFS from the In-As nearest-neighbor bonds with predicted bond lengths of 2.576 Å . The polarization dependence was included in the model calculation which takes into

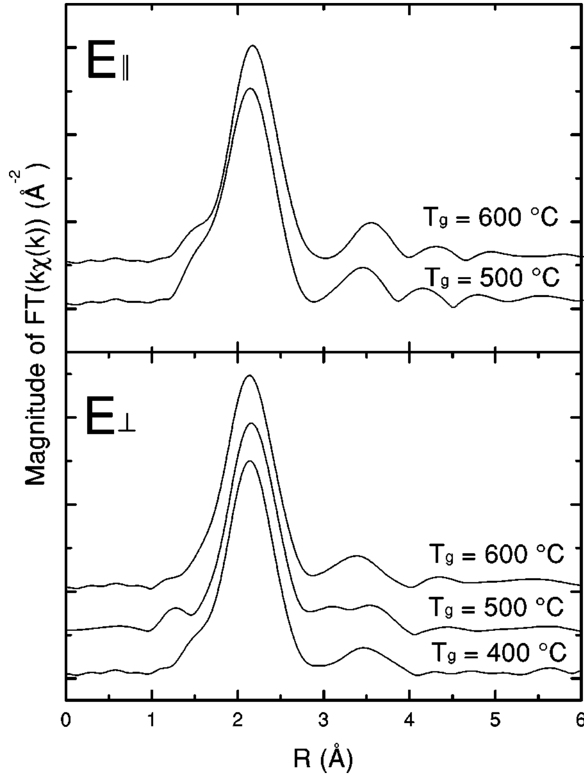

FIG. 12. Fourier transform magnitudes for In *K*-edge XAFS in $E_{\parallel}$ (top curves) and $E_{\perp}$ polarizations (bottom curves) for 1-ML samples and growth temperatures as indicated. The spectra were offset for clarity.

account the $\cos^2(\theta_i)$ dependence. For the $E_{\parallel}$ and $E_{\perp}$ orientations the electric vectors were aligned along the (110) and (001) crystal axes, respectively. In the former geometry the number of As nearest neighbors contributing to the XAFS is 2, while for the latter all 4 neighboring As atoms are expected to contribute.[46]

The Fourier-filtered first shell data for the 1-ML samples, corresponding to the In-As bond lengths, were fitted using the theoretical amplitude $B_i(k)$ and phase $2\delta(k)+\phi_i(k)$. In the fits the variable parameters were S_0^2, R, σ^2 and ΔE_0, which allows for an offset between the theoretical and experimental values of E_0. The fits were carried out using only the data for $k>4$ Å^{-1} to minimize the effect of such an energy shift on the In-As bond length, which is most sensitive to such a discrepancy.

The same fitting procedure was carried out for the InAs reference powder using a FEFF model for InAs. The results are shown in Table II from which it is seen that the theory provides an excellent description of the experimental data for the In-As bond length ($R=2.623$ Å).[47]

Results of the fitting for the 1-ML samples are also shown in Table II. In all cases the experimental values for the In-As bond length are found to agree with the expected value ($R=2.576$ Å) within the uncertainties in the fitting. Similar results were obtained by Woicik *et al.*, working at the In L_3-edge.[2] In that case the *k*-space range was limited to 4 →7.2 Å^{-1} by the intervening L_2-edge. The *K*-edge measurements presented here have the advantage of an extended range in *k*-space which gives higher precision. In addition to the FEFF fits, the present data were also fitted using the InAs reference $\chi(k)$ as an empirical phase, $\phi(k)$, and amplitude, $|f(k)|$, standard,

$$\chi(k)=N^e|f(k)|\sin[2kR^e+\phi(k)]. \tag{15}$$

In this case the variable parameters in the fits were the coordination number, N^e, the In-As bond length, R^e, and an offset ΔE_0. The results are given in Table II.

The bond lengths obtained using the empirical method agree very well with those obtained using the theoretical calculation. There does not appear to be any connection between the In-As bond lengths and the growth temperature.

If each sample consisted of In atoms arranged in single layers, then the XSW results might be interpreted in terms of reduced bond length compression at lower values of T_g. Assuming coherency with the GaAs substrate, the experimental values of P^H would then correspond to In-As bond lengths of $R=2.612$ Å (400 °C), $R=2.594$ Å (500 °C) and $R=2.576$ Å (550,600 °C). Clearly the XAFS bond lengths do not support this single-layer interpretation for the lower values of T_g.

D. Comparison between structural and optical properties

The PL spectra for the 1-ML samples are shown in Fig. 13. For the sample grown at 400 °C the spectrum shows very weak In-excitonic luminescence. The feature labeled ''DAP'' represents donor-acceptor pair (1.490 eV) and free-to-bound (1.493 eV) transitions at carbon impurities. These result from the incomplete decomposition of TBA's precursor molecules, leading to carbon incorporation in the crystal. For the remaining samples, the PL emission energies increase with growth temperature, while the linewidths generally decrease. An exception is the sample with $T_g=530$ °C, exhibiting particularly narrow and bright luminescence. The inhomogeneity of the peak shift could be due to slight dif-

TABLE II. Experimental In-As bond lengths determined from the XAFS analysis for the 1-ML samples. The results obtained using Feff and the empirical standard are presented.

Mode	Sample	R (Å)	R^e (Å)
Transmission	InAs	2.625±0.004	
$E_{\parallel}$	500 °C	2.571±0.007	2.568±0.006
	600 °C	2.575±0.004	2.573±0.008
$E_{\perp}$	400 °C	2.574±0.006	2.571±0.007
	500 °C	2.585±0.008	2.581±0.008
	600 °C	2.571±0.006	2.567±0.009

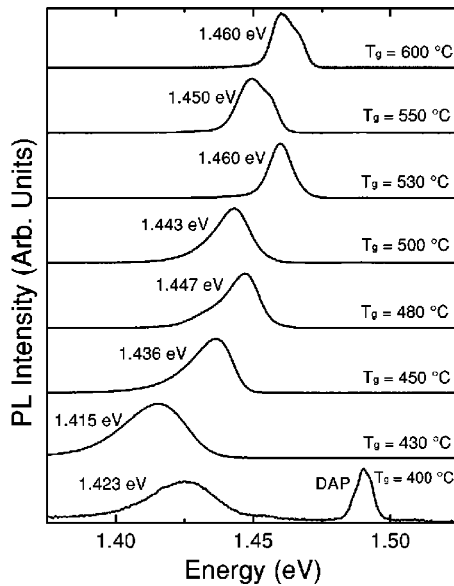

FIG. 13. Photoluminescence spectra for a series of 1-ML InAs samples, with growth temperatures as indicated. The spectra were normalized to a peak height of unity and offset for clarity.

ferences in the amount of incorporated In, or subtle differences in the layer morphologies.

For the $\frac{1}{2}$-ML samples (Fig. 14), 400 °C is again seen to be unsuitable for good optical material, despite the more promising XSW results. The spectrum is dominated by the carbon impurity features. The brightest $\frac{1}{2}$-ML In-luminescence is observed for the sample with $T_g = 600\,^{\circ}\mathrm{C}$.

A comparison between the structural and optical properties appears in Fig. 15. The data suggest a correspondence between the decreasing coherent position and the increasing PL peak energies as a function of growth temperature in the 1-ML samples. As well, the PL linewidths decrease dramatically with increasing growth temperature. This is mirrored somewhat by the increasing coherent fraction. These characteristics may be attributed to a trend towards more perfect, δ-like InAs layers, being particularly evident in the 530–550 °C range.

Previous treatments[23] of the effect of In segregation on optical emission found that with decreasing growth temperature the transition energies are shifted towards lower energies and then saturate at minima which, the authors argued, correspond to minima of segregation. In that case, however, the transition energy vs T_g curves were concave up. From Fig. 15, our results do not reproduce these observations. Rather, the PL energies increase with increasing T_g, and may approach limiting behavior at temperatures beyond those considered here. We point out that the curve is concave down in this case. Thus, these results do not necessarily indicate temperature-dependent segregation.

Previously in this paper we showed that the large coherent positions observed by XSW in the low-T_g samples were consistent with model (ii) which supposed In incorporation in islands rather than in graded $In_xGa_{1-x}As$ layers. If the lateral extent of these islands is greater than the exciton radius, then the net effect would be a decrease in the emission energy due to the fact that the exciton samples a potential well of thickness significantly greater than 1 ML, while maintaining an average layer thickness of approximately 1 ML.[10,12]

These data could also be related to excess In in the samples grown at the lowest temperatures, according to the discussion accompanying Fig. 9.

The lack of any clear trend for the $\frac{1}{2}$-ML samples is noteworthy; since the MOVPE InAs growth exposures for these samples were half the corresponding values for the full ML's, we might expect similarities between the two series. The lack thereof may be related to details of the growth mechanism at the subML scale. For example, the growth could take place in either two-dimensional or three-dimensional modes, or could involve compositional alloying, the details of which are difficult to resolve.

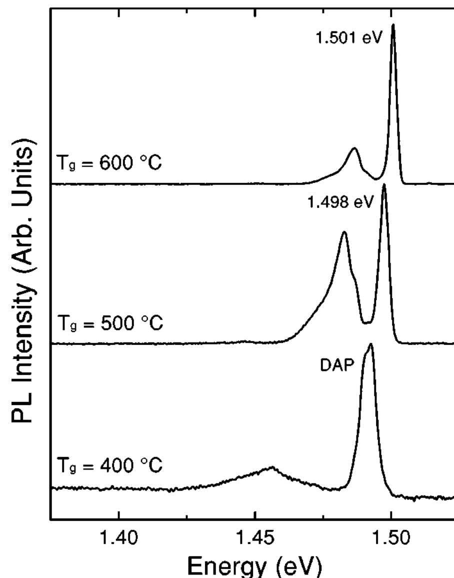

FIG. 14. Photoluminescence spectra for a series of $\frac{1}{2}$-ML InAs samples, with growth temperatures as indicated. The spectra were normalized to a peak height of unity and offset for clarity.

IV. CONCLUSIONS

We have used x-ray standing waves, x-ray diffraction, polarization-dependent XAFS, and PL to assess the structural perfection and the light-emitting characteristics of monolayer and submonolayer InAs quantum wells in GaAs, prepared by MOVPE. Structurally, the best 1-ML sample has been realized at 550 °C according to the agreement between the data and the expected coherent position for the In layer, and the relatively high coherent fraction. The first-neighbor In-As bond lengths determined from the XAFS agree with the macroscopic description of the strain accommodation. The variation in the experimental XSW parameters with growth temperature has been compared with a model for the segregation of In atoms into islands during the GaAs caplayer growth. To our knowledge, this is the first time that the segregation effect has been studied in samples prepared by MOVPE. Our measurements suggest that in the mass-transport-limited regime the MOVPE growth conditions are successful in limiting the deleterious effects of segregation. Additionally, we find a correlation between the XSW results and the PL emission energies and linewidths. These experiments show that the layers with the highest structural quality also exhibit the best optical properties.

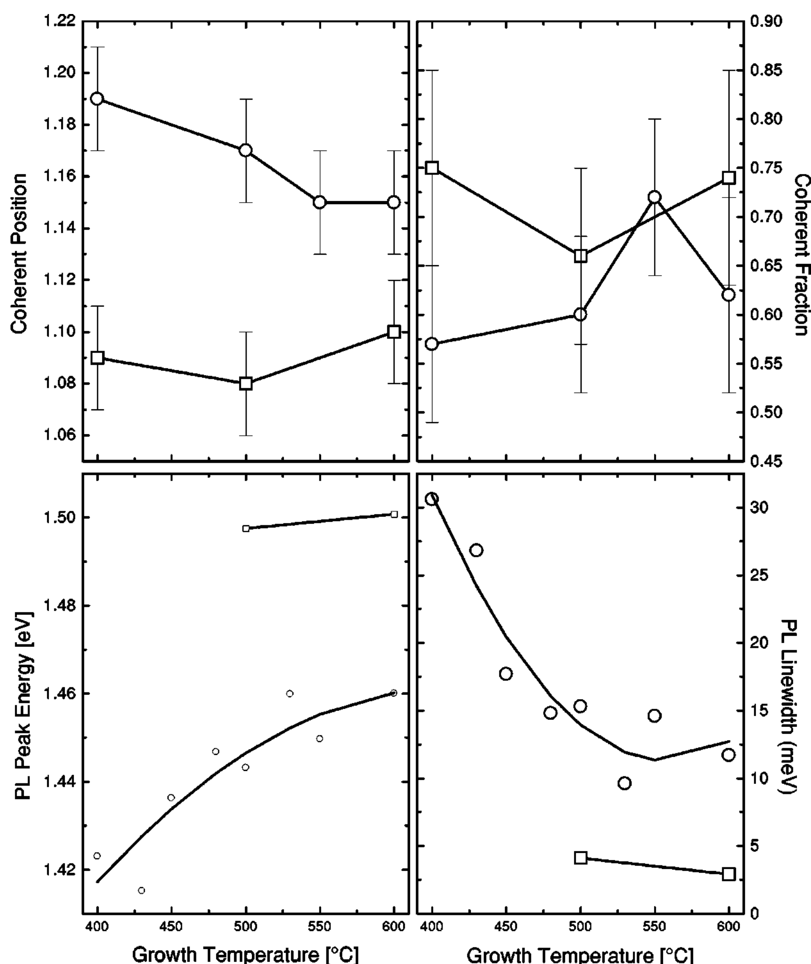

FIG. 15. Summary of the XSW and PL results for all samples. The circles and squares correspond to 1-ML and $\frac{1}{2}$-ML samples, respectively. For the PL data, the uncertainties are given approximately by the symbol size. The solid lines are guides for the eye.

ACKNOWLEDGMENTS

This research was funded by the Natural Sciences and Engineering Research Council of Canada. The National Synchrotron Light Source is funded by the U.S. Department of Energy under Contract No. DE-AC02-76CH00016. The Stanford Synchrotron Radiation Laboratory is funded by the U.S. Department of Energy, Office of Basic Energy Sciences, Divisions of Chemical and Materials Science, and the Office of Biological and Environmental Research. The SSRL Biotechnology Program is supported by the National Institutes of Health, National Center for Research Resources, Biomedical Technology Program.

*Present address: National Research Council of Canada, Institute for Microstructural Sciences, Ottawa, Ontario, Canada, K1A0R6.
†Present address: N&K Technology, 3150 De La Cruz Blvd, Santa Clara, California 95054.

[1] C. Giannini, L. Tapfer, S. Lagomarsino, J.C. Bouillard, A. Taccoen, B. Capelle, M. Ilg, O. Brandt, and K.H. Ploog, Phys. Rev. B **48**, 11 496 (1993).
[2] J.C. Woicik, J.G. Pellegrino, S.H. Southworth, P.S. Shaw, B.A. Karlin, C.E. Bouldin, and K.E. Miyano, Phys. Rev. B **52**, R2281 (1995).
[3] T.-L. Lee, Y. Qian, P.F. Lyman, J.C. Woicik, J.G. Pellegrino, and M.J. Bedzyk, Physica B **221**, 437 (1996).
[4] J.C. Woicik, K.E. Miyano, J.G. Pellegrino, P.S. Shaw, S.H. Southworth, and B.A. Karlin, Appl. Phys. Lett. **68**, 3010 (1996).
[5] J.A. Gupta, J.C. Woicik, S.P. Watkins, K.E. Miyano, J.G. Pellegrino, and E.D. Crozier, J. Cryst. Growth **195**, 34 (1998).
[6] O. Brandt, L. Tapfer, R. Cingolani, K. Ploog, M. Hohenstein, and F. Phillip, Phys. Rev. B **41**, 12 599 (1990); O. Brandt, K. Ploog, L. Tapfer, M. Hohenstein, R. Bierwolf, and F. Phillip, *ibid.* **45**, 8443 (1992).
[7] M.V. Belousov, N.N. Ledentsov, M.V. Maximov, P.D. Wang, I.N. Yasievich, N.N. Faleev, I.A. Kozin, V.M. Ustinov, P.S. Kop'ev, and C.M. Sotomayor Torres, Phys. Rev. B **51**, 14 346 (1995).
[8] M.I. Alonso, M. Ilg, and K.H. Ploog, Phys. Rev. B **50**, 1628 (1994).
[9] W. Li, Z. Wang, J. Liang, B. Xu, Z. Zhu, Z. Yuan, and J. Li, Appl. Phys. Lett. **67**, 1874 (1995).
[10] C.A. Tran, R.A. Arés, V.A. Karasyuk, S.P. Watkins, G. Letourneau, and R. Leonelli, Phys. Rev. B **55**, 4633 (1997).
[11] Z.L. Yuan, Z.Y. Xu, B.Z. Zheng, J.Z. Xu, S.S. Li, W. Ge, Y. Wang, J. Wang, L.L. Chang, P.D. Wang, C.M. Sotomayor Torres, and N.N. Ledentsov, Phys. Rev. B **54**, 16 919 (1996).
[12] R.C. Iotti, L.C. Andreani, and M. Di Ventra, Phys. Rev. B **57**, R15 072 (1998).
[13] A.R. Goñi, M. Stroh, C. Thomsen, F. Heinrichsdorff, V. Türck, A. Krost, and D. Bimberg, Appl. Phys. Lett. **72**, 1433 (1998).
[14] C. Guille, F. Houzay, J.M. Moison, and F. Barthe, Surf. Sci. **189**, 1041 (1987).

[15] J.M. Moison, C. Guille, F. Houzay, F. Barthe, and M. Van Rompay, Phys. Rev. B **40**, 6149 (1989).
[16] M. Sato and Y. Horikoshi, Surf. Sci. **267**, 195 (1992).
[17] J.M. Gérard and J.Y. Marzin, Phys. Rev. B **45**, 6313 (1992).
[18] K. Muraki, S. Fukatsu, Y. Shiraki, and R. Ito, Appl. Phys. Lett. **61**, 557 (1992).
[19] T. Kawai, H. Yonezu, Y. Ogasawara, D. Saito, and K. Pak, in *Common Themes and Mechanisms of Epitaxial Growth*, edited by P. Fuoss, J. Tsao, D.W. Kisker, A. Zangwill, and T.F. Kuech, MRS Symposia Proceedings No. 312 (Materials Research Society, Pittsburgh, 1993), p. 113.
[20] M. Larive, J. Nagle, J.P. Landesman, X. Marcadet, C. Mottet, and P. Bois, J. Vac. Sci. Technol. B **11**, 1413 (1993).
[21] K. Muraki, S. Fukatsu, Y. Shiraki, and R. Ito, J. Cryst. Growth **127**, 546 (1993).
[22] J. Nagle, J.P. Landesman, M. Larive, C. Mottet, and P. Bois, J. Cryst. Growth **127**, 550 (1993).
[23] A. Bosacchi, F. Colonna, S. Franchi, P. Pascarella, P. Allegri, and V. Avanzini, J. Cryst. Growth **150**, 185 (1995).
[24] R.A. Arés, C.A. Tran, and S.P. Watkins, Appl. Phys. Lett. **67**, 1576 (1995).
[25] K. Yamaguchi, T. Okada, and F. Hiwatashi, Appl. Surf. Sci. **117**, 700 (1997).
[26] P. Disseix, J. Leymarie, A. Vasson, A.-M. Vasson, C. Monier, N. Grandjean, M. Leroux, and J. Massies, Phys. Rev. B **55**, 2406 (1997).
[27] W.J. Bartels, J. Hornstra, and D.J.W. Lobeek, Acta Crystallogr., Sect. A: Found. Crystallogr. **42**, 539 (1986).
[28] J. Hornstra and W.J. Bartels, J. Cryst. Growth **44**, 513 (1978).
[29] A review article: J. Zegenhagen, Surf. Sci. Rep. **18**, 199 (1993).
[30] D.P. Woodruff, D.L. Seymour, C.F. McConville, C.E. Riley, M.D. Crapper, N.P. Prince, and R.G. Jones, Surf. Sci. **195**, 237 (1988).
[31] R. Saravanan, S.K. Mohanlal, and K.S. Chandrasekaran, Acta. Crystallogr. Sect. A: Found Crystallogr. **48**, 4 (1992).
[32] The depth sensitivity of the fluorescent photons is discussed in Ref. 3. In the present experiment, the average takeoff angle viewed by the detector aperture is greater than the critical angle (1.5° at 1282 eV), and so the FLY includes contributions from atoms at depths of hundreds of angstroms below the surface.
[33] J.C. Woicik, T. Kendelewicz, K.E. Miyano, P.L. Cowan, C.E. Bouldin, B.A. Karlin, P. Pianetta, and W.E. Spicer, Phys. Rev. Lett. **68**, 341 (1992).
[34] J.C. Mikkelsen, Jr. and J.B. Boyce, Phys. Rev. Lett. **49**, 1412 (1982).
[35] J.C. Woicik, J.A. Gupta, S.P. Watkins, and E.D. Crozier, Appl. Phys. Lett. **73**, 1269 (1998).
[36] O. Dehaese, X. Wallart, and F. Mollot, Appl. Phys. Lett. **66**, 52 (1995).
[37] J.A. Gupta, J.C. Woicik, J.G. Pellegrino, K.E. Miyano, E.D. Crozier, and S.P. Watkins (unpublished).
[38] G.B. Stringfellow, *Organometallic Vapor-Phase Epitaxy* (Academic Press, San Diego, CA, 1989).
[39] J.A. Gupta, S.P. Watkins, R. Arés, and G. Soerensen, J. Cryst. Growth **195**, 205 (1998).
[40] J.A. Gupta and S.P. Watkins (unpublished).
[41] S.P. Watkins, C.A. Tran, G. Soerensen, H.D. Chueng, R.A. Ares, Y. Lacroix, and M.L.W. Thewalt, J. Electron. Mater. **24**, 1583 (1995).
[42] M. Newville, P. Livins, Y. Yacoby, J.J. Rehr, and E.A. Stern, Phys. Rev. B **47**, 14 126 (1993).
[43] The data for the standard were obtained in transmission at beamline X23A2 at the NSLS using Si(311) monochromator crystals.
[44] E.A. Stern, in *X-Ray Absorption, Principles, Applications, Techniques of EXAFS, SEXAFS and XANES*, edited by D.C. Koningsberger and R. Prins (Wiley, New York, 1988).
[45] S.I. Zabinsky, J.J. Rehr, A. Ankudinov, R.C. Albers, and M.J. Eller, Phys. Rev. B **52**, 2995 (1995).
[46] J.C. Woicik, C.E. Bouldin, K.E. Miyano, and C.A. King, Phys. Rev. B **55**, 15 386 (1997).
[47] The quoted uncertainties indicate the values that double the squared residuals in each parameter when all other values were allowed to float.